NREL/TP-413-21405 • UC Category: 1263 • DE96007922

Infrared Spectroscopic, X-Ray, and Nanoscale Characterization of Strontium Titanate Thin Films

J. D. Webb, H. R. Moutinho,
L. L. Kazmerski, C. H. Mueller,
T. V. Rivkin, R. E. Treece, M. Dalberth,
and C. T. Rogers

Presented at the 8th ISIF (International Symposium on Integrated Ferroelectrics), March 17–20, 1996, Tempe, Arizona

Revision of NREL/TP-413-20926

National Renewable Energy Laboratory
1617 Cole Boulevard
Golden, Colorado 80401-3393
A national laboratory of
the U.S. Department of Energy
Managed by Midwest Research Institute
for the U.S. Department of Energy
under contract No. DE-AC36-83CH10093

Prepared under Task No. 0841.2001

June 1996

NOTICE

Available to DOE and DOE contractors from:
Office of Scientific and Technical Information (OSTI)
P.O. Box 62
Oak Ridge, TN 37831
Prices available by calling (423) 576-8401

Available to the public from:
National Technical Information Service (NTIS)
U.S. Department of Commerce
5285 Port Royal Road
Springfield, VA 22161
(703) 487-4650

Printed on paper containing at least 50% wastepaper, including 10% postconsumer waste

INFRARED SPECTROSCOPIC, X-RAY, AND NANOSCALE CHARACTERIZATION OF STRONTIUM TITANATE THIN FILMS

J. D. Webb, H. R. Moutinho, L. L. Kazmerski
National Renewable Energy Laboratory, Golden, CO 80401

C. H. Mueller, T. V. Rivkin, and R. E. Treece
Superconducting Core Technologies, Inc., Golden, CO 80401

M. Dalberth and C. T. Rogers
Department of Physics, University of Colorado, Boulder, CO 80309

Abstract Attenuated total reflectance (ATR) measurements were performed using Fourier transform infrared (FTIR) spectroscopy in the ATR mode with a thallium iodobromide (KRS-5) crystal to measure the frequencies of the ν_3 and ν_4 phonon absorption bands in thin strontium titanate films deposited on single-crystal yttrium-barium copper oxide (YBCO), lanthanum aluminate, magnesium oxide, and strontium titanate substrates. The KRS-5 crystal enabled FTIR-ATR measurements to be made at frequencies above 400 cm^{-1}. Atomic force microscopy (AFM) and X-ray diffraction (XRD) measurements were also made to further characterize the films. The measurements were repeated on single-crystal specimens of strontium titanate and the substrates for comparison. Softening in the frequency of the ν_4 transverse optical phonon in the lattice-mismatched films below the established value of 544 cm^{-1} is indicative of the highly textured, polycrystalline ceramic nature of the films and is consistent with the XRD and AFM results.

INTRODUCTION

Infrared (IR) absorption and Raman scattering techniques were instrumental in uncovering the origins of ferroelectric behavior in bulk perovskite materials such as strontium titanate (STO) and barium titanate (BTO).[1-9] The temperature dependence of the real portion of the dielectric constant, ϵ_r, at low (microwave) frequencies is associated with ferroelectric behavior. The spectroscopic techniques confirmed that the temperature dependence of ϵ_r is related to temperature-dependent shifts in the frequency, ν_1, of the low-frequency transverse optic (TO) phonon (higher-frequency phonons do not shift significantly with temperature).[6] The relationship between the dielectric constants and the set of j phonon frequencies is given by the Lyddane, Sachs, Teller equation: [6,10,11]

$$\frac{\epsilon_0(T)}{\epsilon_\infty} = \frac{\omega_{l1}^2}{\omega_{t1}^2}\frac{\omega_{l2}^2}{\omega_{t2}^2} \cdots \frac{\omega_{lj}^2}{\omega_{tj}^2}, \qquad [1]$$

where $\epsilon_0(T)$ is the low-frequency dielectric constant, ϵ_∞ is the dielectric constant at optical frequencies, ω_{Tj} is the frequency of the jth transverse optical phonon, and ω_{Lj} is the frequency of the jth longitudinal optical (LO) phonon. The normal mode vibration

associated with the ν_1 optical phonon is a motion of the TiO_6 octohedra relative to the strontium cations; the j = 2 and higher phonons are associated with bending and stretching vibrations of the TiO_6 octohedra.[1,3]

The "softening" of the ν_1 TO vibration mode to lower frequencies as the material approaches the Curie temperature creates a large difference in frequencies between ω_{T1} and ω_{L1}, thus ϵ_0 (T) increases at low temperatures.[2] Subsequent papers have also shown that when the material is paraelectric, applying a DC electric field suppresses the softening of the ν_1 vibration mode, thus the dielectric constant is reduced.[11]

Despite the clear correlations established between IR properties and dielectric response in bulk perovskites, our review of the available literature discovered no citations giving the IR absorbance spectra of STO or any other perovskite thin film. We suspect that the IR spectra of epitaxial perovskite films have not been widely reported because most of the substrates that are suitable for growing epitaxial STO films (e.g. lanthanum aluminate [LAO], Al_2O_3, MgO) strongly absorb and poorly reflect IR radiation at frequencies less than 700 cm^{-1}. This substrate absorption would obscure the much weaker absorption of the thin epitaxial film at these frequencies if conventional transmission or refection methods were used in attempts to measure the film spectra.

To measure the IR absorption spectra characteristic of the ν_3 and ν_4 lattice modes of highly textured STO films, as well as substrate lattice modes, we used ATR spectroscopy. In ATR spectroscopy, the sample is pressed against an IR waveguide that has a higher refractive index than the sample.[12] In this work, we used a waveguide fabricated from thallium iodobromide (KRS-5), which has a refractive index of 2.4 and is transparent from 14,000 cm^{-1} to 400 cm^{-1}.[12] Most of the IR radiation is internally reflected at the KRS-5/STO interface and propagates through the KRS-5 crystal. However, an evanescent wave that propagates into the STO/substrate samples is associated with the internally reflected radiation. Because the penetration depth of the evanescent wave is typically only a few times the thickness of the STO films on the nonconductive substrates, the IR absorption spectra of both the thin films and the insulating substrates were readily obtained by using this technique.

The films were deposited in-situ at 750°-800° C using pulsed-laser ablation of a ceramic target. The STO, LAO, and MgO substrates were (100)-oriented single crystals, and the atomic force microscopy (AFM) and X-ray diffraction (XRD) measurements (Figures 1 and 2, respectively) show that the STO films were highly textured, (100)-oriented epitaxial layers with grain sizes of 50-100 nm. The contact-mode AFM measurements were done with silicon cantilevers in ambient air using an Autoprobe Model LS atomic force microscope manufactured by Park Scientific Instruments, Inc. The XRD data were obtained from a standard $\theta/2\theta$ diffractometer attached to a Rigaku rotating copper anode generator. The copper K_α radiation was selected by a graphite monochromator. The YBCO substrates were (001)-oriented films on LAO, which are sufficiently conductive to be highly IR-reflective at room temperature, enabling FTIR spectroscopy in the reflection-absorbance (RA) mode,[13] as well as FTIR-ATR spectroscopy to be done on the STO/YBCO sample. The nominal thickness, d, of the STO films was 500 nm.

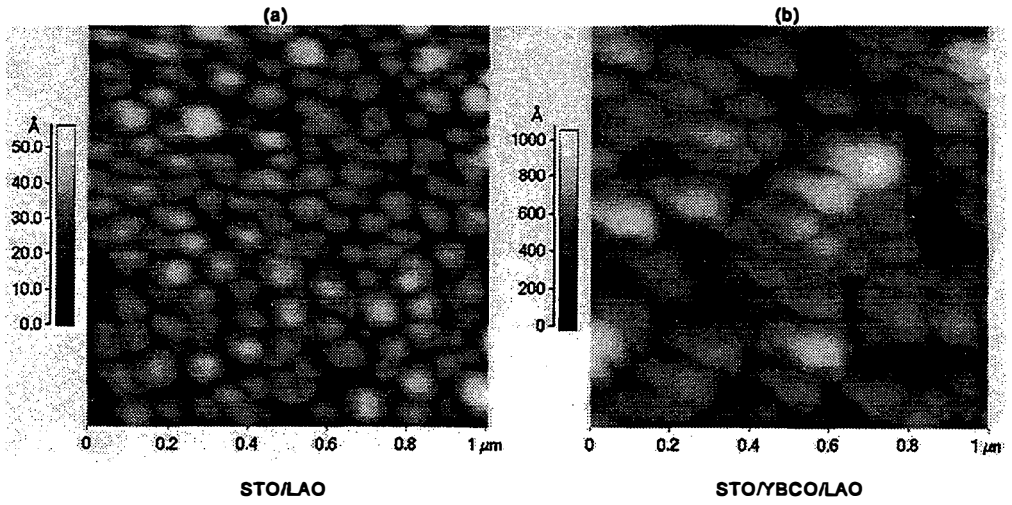

Figure 1. Atomic force micrographs of STO film on LAO (a), and STO film on YBCO/LAO (b).

The FTIR-RA spectra were collected without polarization using a Nicolet Corp. Magna 550 FTIR spectrophotometer with a Spectra-Tech FT-30 specular reflectance attachment at 30 degrees incidence angle. The FTIR-ATR spectra were collected at 45 degrees incidence using a 1-cm x 0.5-cm x 0.1-cm thallium iodobromide (KRS-5) ATR crystal, a Perkin-Elmer wire-grid polarizer, and a Nicolet System 800 FTIR spectrophotometer. The resolution for the FTIR measurements was 2 cm^{-1}. A schematic of the configuration for FTIR-ATR spectroscopic measurements is shown in Figure 3.

In ATR spectroscopy, the IR wave must be internally reflected in the waveguide; thus the refractive index n_2 of the adjacent sample must be less than the index n_1 of the ATR crystal. To achieve internal reflection, the angle of incidence, θ, of the IR signal relative to the substrate normal must be greater than

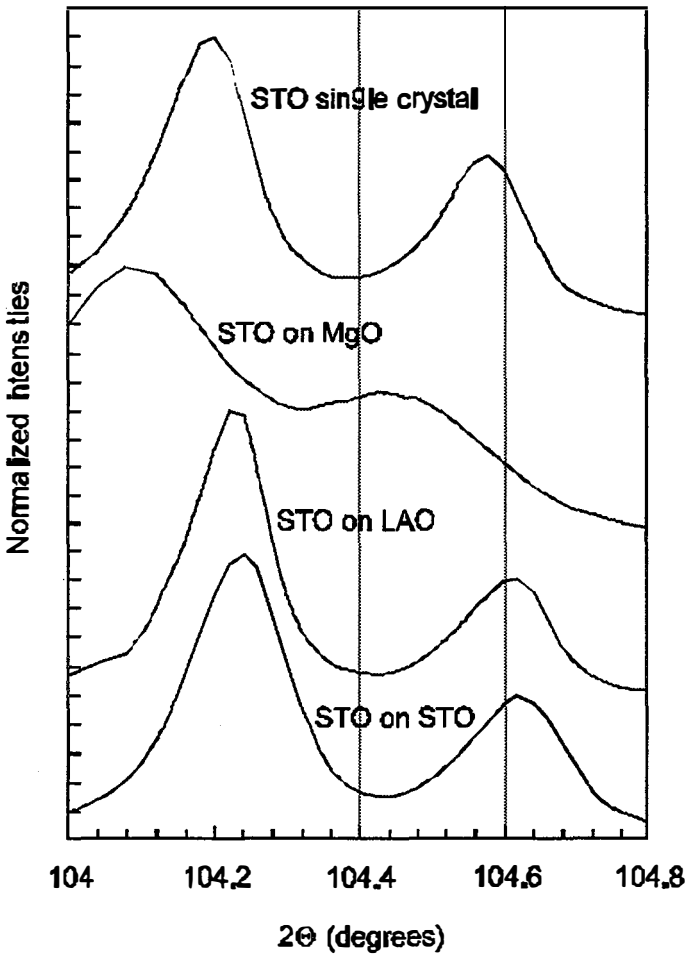

Figure 2. (400) X-ray diffraction patterns of STO single-crystal, STO film on MgO, STO film on LAO, and STO film on STO single-crystal substrate.

the critical angle, θ_c, which is given by:

$$\theta_c = \sin^{-1} n_{21} \quad (n_{21} = n_2/n_1). \qquad [2]$$

For bulk samples with refractive index n_2, the effective penetration depths, d_e, for p-polarized (perpendicular to sample plane) and s-polarized (parallel to sample plane) IR radiation are, respectively:[12]

$$d_{ep} = \frac{n_{21} \cos\theta}{\pi\nu(1 - n_{21}^2)\,(\sin^2\theta - n_{21}^2)^{1/2}} \qquad [3]$$

and

$$d_{es} = \frac{n_{21} \cos\theta\,(2\sin^2\theta - n_{21}^2)}{\pi\nu(1 - n_{21}^2)\,[(1 - n_{21}^2)\sin^2\theta - n_{21}^2]\,(\sin^2\theta - n_{21}^2)^{1/2}}. \qquad [4]$$

Note that d_e approaches infinity as n_{21} approaches unity and θ_c approaches 90 degrees to the sample normal. Optical constants for LAO were taken from Zhang et al,[14] while those for MgO and STO were taken from Palik.[15]

For films that are thin relative to the evanescent wave penetration depth, d_p, it is only necessary that the refractive index n_3 of the substrate, and not necessarily that of the film, n_2, be less than the refractive index n_1 of KRS-5 for internal reflection to occur. For films such as STO of thickness $d \ll d_p$ on substrates as shown in Figure 3, the effective penetration depths, d_e, for the p-polarized and s-polarized IR radiation are, respectively: [12]

$$d_{ep} = \frac{4\, n_{21}\, d \cos\theta}{(1 - n_{31}^2)} \qquad [5]$$

and

$$d_{es} = \frac{4\, n_{21}\, d \cos\theta[(1 + n_{32}^4)\sin^2\theta - n_{31}^2]}{(1 - n_{31}^2)\,[(1 + n_{31}^2)\sin^2\theta - n_{31}^2]} \qquad [6]$$

Note that in the thin-film case (eqs. 5 and 6), d_e is independent of the frequency ν of the incident IR radiation, and that d_e approaches infinity and θ_c approaches 90 degrees as n_{31} approaches unity. The results of calculations for d_{ep} and d_{es} of an evanescent wave extending from a KRS-5 waveguide into STO and LAO substrates, and into STO/LAO samples for $\theta = 45°$ over the spectral range, 800-400 cm^{-1}, within which the STO ν_3 and ν_4 absorbances are observed, are summarized in Figure 4. The spectral ranges given in Figure 4 are those in which d_e is finite. For MgO substrates and STO/MgO samples, d_e is finite between 800 cm^{-1} and 405 cm^{-1}. STO films on STO substrates behave like STO substrates, i.e., eqs. 3 and 4 apply. For STO/YBCO samples, the conductivity of the YBCO film implies that $d_e = d$.

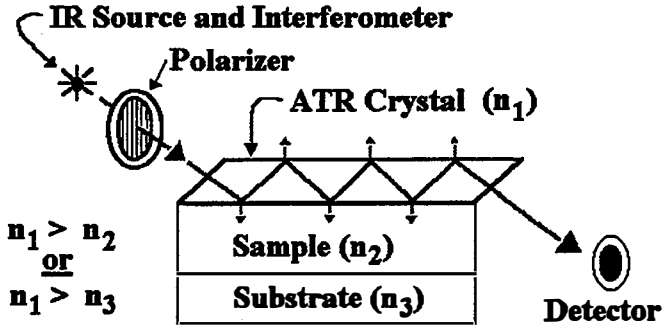

Figure 3. ATR spectroscopy configuration

RESULTS AND DISCUSSION

The peak frequencies of the absorbance bands measured using FTIR-ATR spectroscopy of the various samples are summarized in Table I.

TABLE I. Frequencies of ATR-FTIR peak maxima compared with (reported) values for the lattice frequencies in the samples analyzed.

	Material						
Mode	LAO	MgO	STO	STO/ YBCO	STO/ LAO	STO/ MgO	STO/ STO
ω_{t1}	(184)[14]	(396)[15]	(86)[6]				
ω_{l1}	(350)[14]	591 (590)[15]	(173)[6]				
ω_{t2}	- (428)[14]	643 (643)[15]	(176)[6]				
ω_{l2}	562 (560)[14]	- (730)[15]	(265)[6]		- /604		
ω_{t3}	495 (496)[14]		(265)[6]		- /495		
ω_{l3}	-		455 (473)[6]	471/ -	468/ -	469/ -	449/ -
ω_{t4}	636 (657)[14]		505 (544)[6]	538/ -	530/636	532/ -	505/ -
ω_{l4}	686 (710)[14]		- (804)[6]	752/ -	779/ -	785/ -	

Note that the STO phonons at 265 cm^{-1} are IR-inactive.[6]

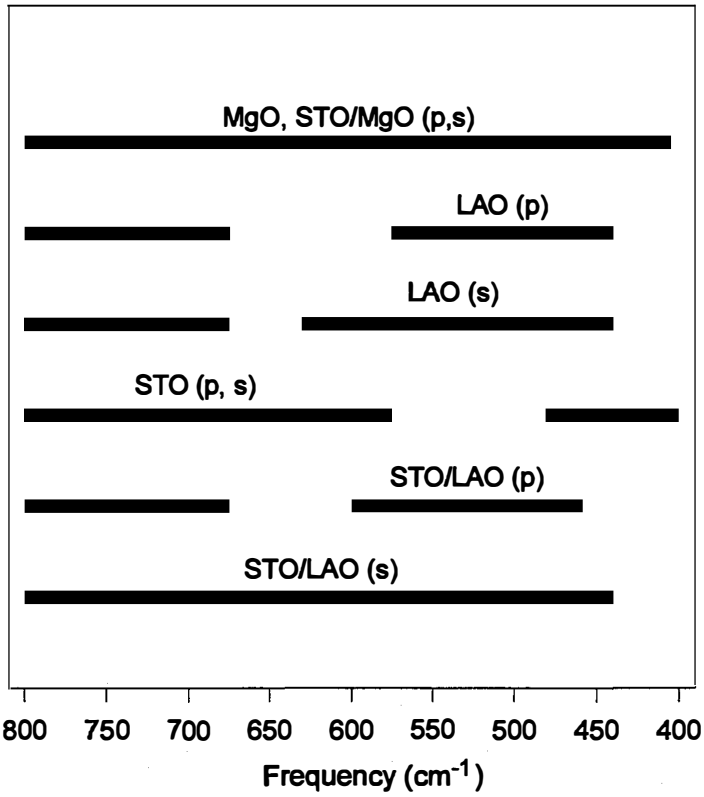

Figure 4. Frequency ranges for finite d_e.

The frequencies of the FTIR-ATR absorption maxima for the thin STO films are significantly softened relative to the frequencies expected for single-crystal STO.[6] The frequency shifts observed were significant with respect to the resolution (2 cm^{-1}) of the FTIR spectrophotometer. This observation is consistent with the polycrystalline nature of the films as determined by AFM and XRD measurements (Figures 1 and 2). Similar shifts have been observed in the Raman spectra of amorphous lead titanate as it is annealed through a locally ordered partially crystallized state to a highly crystalline state exhibiting long-range ordering.[16] The softening is greater for STO films on LAO than for STO films on YBCO, which exhibit larger surface grain sizes and are less uniform (Figure 1). The minimum, mean, and maximum grain sizes for the STO/LAO film, determined from visual inspection of Figure 1a, are 57, 91, and 118 nm, respectively. A similar analysis of the data in Figure 1b gives minimum, mean, and maximum grain sizes of 72, 112, and 185 nm for the STO/YBCO film. The differences are significant, especially if grain volume, which presumably influences the phonon frequencies, is related to a power of the surface grain size observed for the films. The FTIR-ATR spectra of STO/LAO and of STO samples are given in Figures 5 and 6. The FTIR-ATR spectra of an STO/YBCO sample is given in Figure 7.

The ν_4 TO mode of the STO film on YBCO at 538 cm^{-1} in Figure 7 is very weak, as expected for a film on a good conductor. This observation confirms that the strong absorbance at 471 cm^{-1} in Figure 7 (STO/YBCO in perpendicular polarization) is attributable to a LO phonon and not to a TO phonon shifted because of thin-film confinement or powder-like film structure.[17] The unpolarized FTIR reflectance spectrum of a similar STO/YBCO sample (Figure 8) shows inverted reflection-absorbance bands characteristic of both TO and LO modes, as expected for IR spectra taken at non-normal incidence.[18] The FTIR-ATR measurements of STO films on LAO (Figures 5 and 6) and MgO (not shown), exhibit stronger ν_4 TO absorption.

As mentioned previously, it is possible to observe several absorbance bands characteristic of the substrates in the FTIR-ATR spectra of the STO/LAO samples, the STO single crystals, and the LAO single crystals. In many cases, the maxima of these bands are

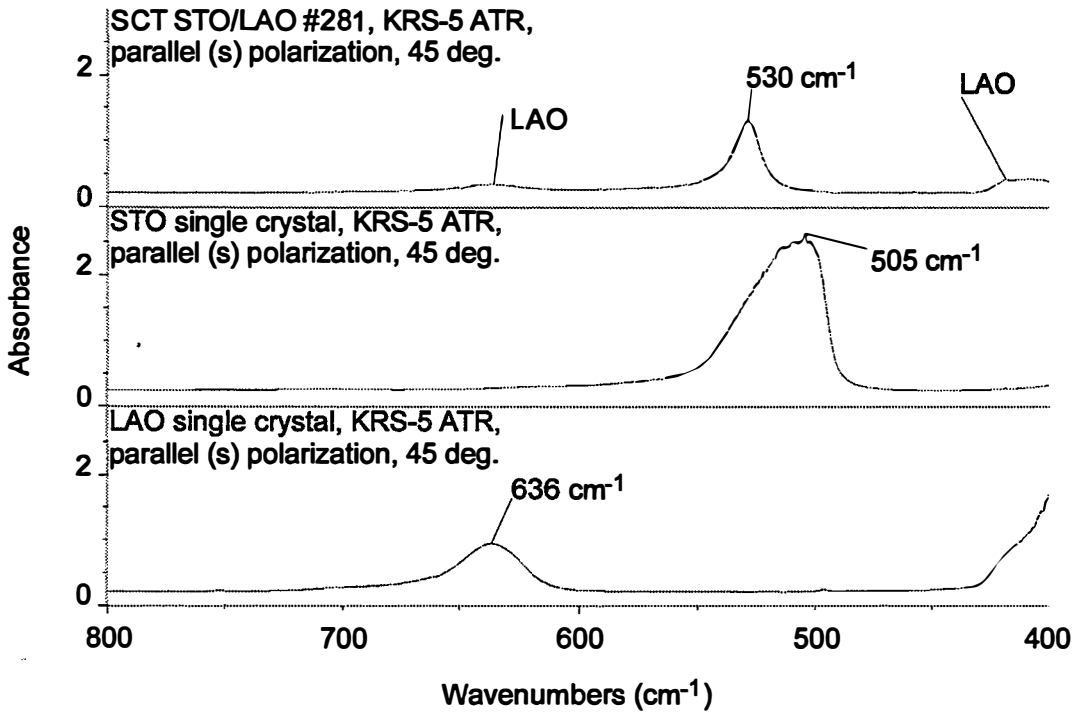

Figure 5. Parallel-polarized FTIR-ATR spectra of STO/LAO, STO, and LAO.

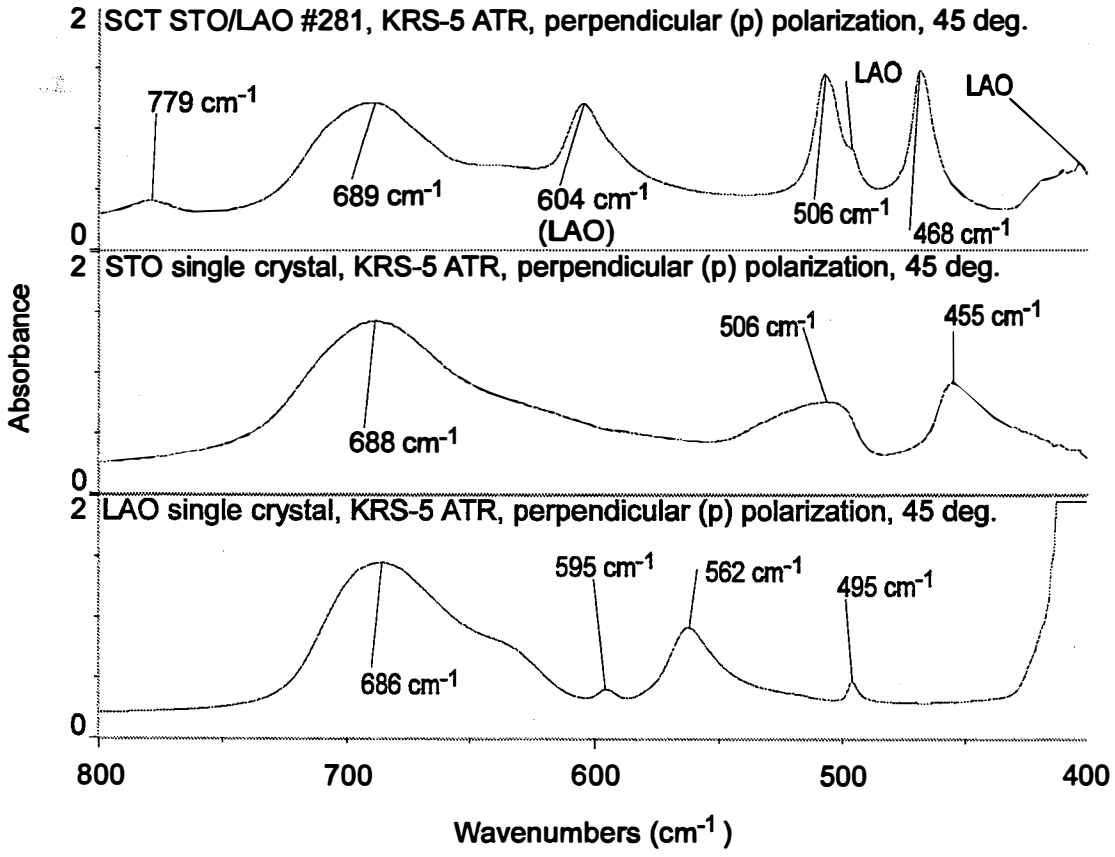

Figure 6. Perpendicular-polarized FTIR-ATR spectra of STO/LAO, STO, and LAO.

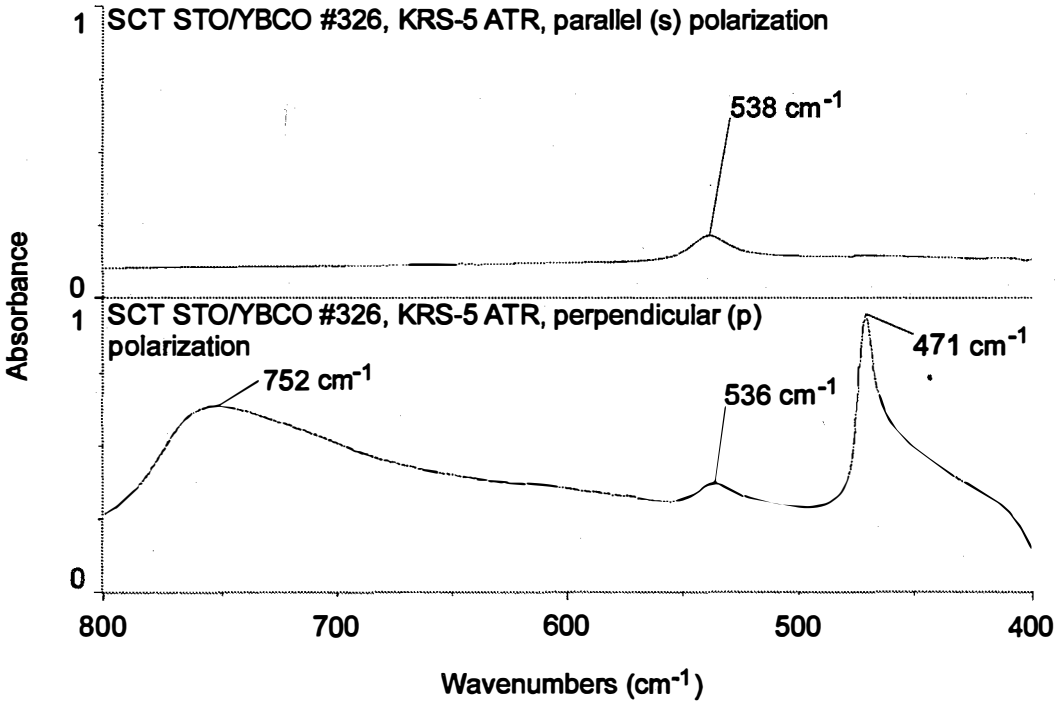

Figure 7. Parallel (p) and perpendicular (s) -polarized FTIR-ATR spectra of STO film on YBCO/LAO substrate.

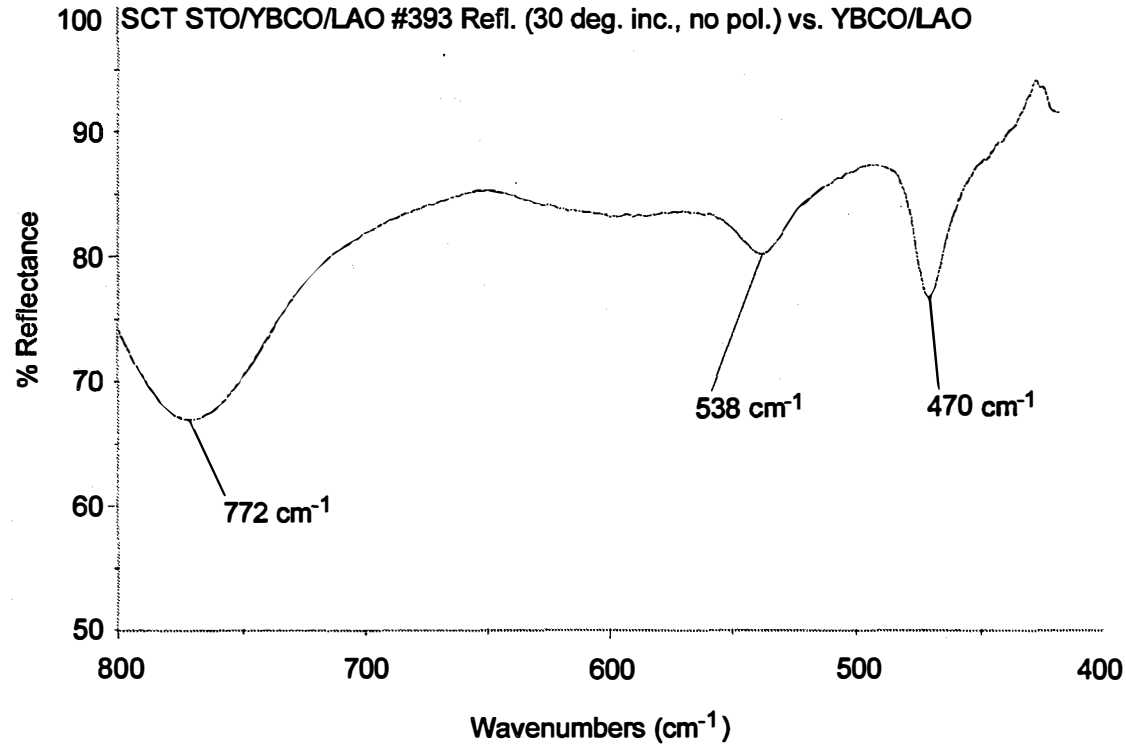

Figure 8. Unpolarized FTIR reflectance spectrum (30 degrees incidence) of STO film on YBCO/LAO substrate showing reflection-absorbance at the STO LO and TO phonon frequencies. A YBCO film deposited onto an LAO substrate was used as a reflectance standard.

significantly shifted relative to the published frequencies for the corresponding lattice modes (Table I). However, with reference to Figure 4, it is interesting to note that the shifted band maxima correspond to frequencies at which d_ϵ approaches infinity (eqs. 3–6). The shifts observed in these bands are apparently optical artifacts. For this reason, the frequencies of maxima in the FTIR-ATR spectra of the thin STO films, which occur in spectral regions where d_ϵ is finite, were compared with the published lattice frequencies for STO rather than to those measured for single-crystal STO using FTIR-ATR spectroscopy (Table I). Little or no shifting of the FTIR-ATR band maxima characteristic of the substrates relative to published values (Table I) is observed in spectral regions where d_ϵ is finite (Figure 4).

Softening of the ω_{t4} mode indicates that this phonon is more heavily damped in STO thin films than in bulk, single crystal STO.[19] However, using XRD, no strain was observed in the STO films on LAO and STO substrates, and STO film on MgO displayed little strain. This indicates that the softening of the ω_{t4} mode was caused by polycrystallinity in the film, and phonon damping (and thus softening) was minimized for films with larger grain sizes. However, the XRD measurements used in these experiments only measured the out-of-plane lattice parameters (normal to the substrate surface); a more comprehensive correlation between lattice strain and phonon damping would require the in-plane as well as out-of-plane lattice parameters to be measured.

The observation that the softening of the higher-frequency ν_3 and ν_4 phonons in STO films is related to the polycrystalline grain size of the films raises the interesting possibility that the ν_1 TO phonon responsible for the ferroelectric behavior of STO may be also softened in the films, a hypothesis that has some support in the literature.[16] Such softening could reduce the temperature dependence of the ν_1 TO phonon frequency and therefore impair the film's ferroelectric properties. Similarly, strain in ferroelectric STO films has been shown to have a significant influence over the temperature dependence of the dielectric constant in STO films[20] and may affect the performance of devices containing such films.

ACKNOWLEDGMENT

We thank Dr. Don Williamson at the Physics Department, Colorado School of Mines (Golden, Colorado) for use of the Rigaku X-ray diffractometer.

REFERENCES

1. J.T. Last, Phys. Rev. 105, pp. 1740-1750 (1957).
2. A.S. Barker, Jr., and M. Tinkham, Phys. Rev. 125, pp. 1527-1530 (1962).
3. W.G. Spitzer, R.C. Miller, D.A. Kleinman, and L.E. Howarth, Phys. Rev. 126, pp. 1710-1721 (1962).
4. R.A. Cowley, Phys. Rev. 134, pp. A981-A997 (1964).
5. A.S. Barker, Jr., and J.J. Hopfield, Phys. Rev. 135, pp. A1732-A1737 (1964).
6. A.S. Barker, Jr., Phys. Rev. 145, pp. 391-399 (1966).
7. W.G. Nilsen and J.G. Skinner, J. Chem. Phys. 48, pp. 2240-2248 (1968).

8. M. DiDomenico, Jr., S.H. Wemple, P.S. Porto, and R.P. Bauman, Phys. Rev. 174, pp. 522-530 (1968).
9. M.S. Jang, K.S. Yi, D.T. Ro, and T. Nakamura, Ferroelectrics 137, pp. 97-104 (1992).
10. R.H. Lyddane, R.G. Sachs, and E. Teller, Phys. Rev. 59, pp. 673-676 (1941).
11. P.A. Fleury and J.M. Worlock, Phys. Rev. Lett. 18, pp. 665-667 (1967).
12. Internal Reflection Spectroscopy, N. J. Harrick, Interscience Div., John Wiley & Sons, New York (1967).
13. H. G. Tompkins, "Infrared Reflection-Absorption Spectroscopy," in Methods of Surface Analysis I, A. W. Czanderna (ed.), Elsevier Co., New York, p. 458 (1975).
14. Z. M. Zhang, B. I. Choi, M. I. Flik, and A. C. Anderson, J. Opt. Soc. Am. B, 11, 11, p. 2252 (1994).
15. Handbook of Optical Constants of Solids II, E. D. Palik (ed.), Academic Press, Inc., Boston (1991).
16. T. Nakamura and M. Takashige, J. Phys. Soc. Jpn. 49, pp. 38-41 (1980).
17. J. T. Luxon, D. J. Montgomery, and R. Summitt, J. Appl. Phys. 41, 6, pp. 2303-2307 (1970).
18. D. W. Berreman, Phys. Rev. 130, 6, p. 2193 (1963).
19. J.C. Burfoot and G.W. Taylor, Polar Dielectrics and Their Applications, University of California Press, Los Angeles, p. 181 (1979).
20. L. A. Knauss, J. S. Horwitz, D. B. Chrisey, J. M. Pond, K. S. Grabowski, S. B. Quadri, E. P. Donovan, and C. H. Mueller, Proc. MRS 388, pp. 73-78 (1995).